EARTH SURFACE PROCESSES AND LANDFORMS
Earth Surf. Process. Landforms (2019)

Published online in Wiley Online Library
(wileyonlinelibrary.com) DOI: 10.1002/esp.4672

Spatiotemporal variations of dissolved inorganic carbon and controlling factors in a small karstic catchment, Southwestern China

Caiqing Qin,[1] Si-Liang Li,[1,2,3]* Fu-Jun Yue,[4] Sheng Xu[1] and Hu Ding[2,3,4]*

[1] Institute of Surface-Earth System Science, Tianjin University, Tianjin 300072, China
[2] State Key Laboratory of Environmental Geochemistry, Institute of Geochemistry, Chinese Academy of Sciences, Guiyang 550081, China
[3] Puding Karst Ecosystem Observation and Research Station, Chinese Academy of Sciences, Puding 562100, China
[4] School of Geographical and Earth Sciences, University of Glasgow, Glasgow G12 8QQ, UK

Received 1 November 2018; Revised 12 May 2019; Accepted 20 May 2019

*Correspondence to: Si-Liang Li, Institute of Surface-Earth System Science, Tianjin University, Tianjin 300072, China. Hu Ding, State Key Laboratory of Environmental Geochemistry, Institute of Geochemistry, Chinese Academy of Sciences, Guiyang 550081, China. E-mail: siliang.li@tju.edu.cn; dinghu@vip.skleg.cn

ESPL
Earth Surface Processes and Landforms

ABSTRACT: Dissolved inorganic carbon (DIC) is the most important carbon component in karst aquatic system where fluid is highly transmissive, but has rarely been examined in the subtropical karst critical zone (K-CZ). In this study, concentrations of dissolved solutes and isotopic compositions of DIC ($\delta^{13}C_{DIC}$) at 11 sites of a 73.4 km^2 karstic catchment in Southwestern China were analysed monthly in order to uncover the spatiotemporal variations of both DIC and its dominant sources, and to identify relevant controlling factors. Both DIC concentrations and $\delta^{13}C_{DIC}$ were highly variable, ranging from 2.52 to 5.85 mmol l^{-1} and from −15.7 to −4.5‰, respectively. DIC in underground water (UGW) was higher in concentration and more depleted in ^{13}C compared to surface water (SFS). DIC concentrations showed an inconsistent seasonal trend with other solutes, with higher values in the wet season at some sites. $\delta^{13}C_{DIC}$ values were lower in the wet season than in the dry season. The results of mixing model IsoSource revealed spatiotemporal patterns of DIC sources. During the dry season, carbonate weathering was the primary contributor to DIC in UGW (excluding in the middle reaches). However, during the wet season, soil CO_2 was the dominant source of DIC in both UGW and SFS, and it was higher than in the dry season. Overall, there are significant spatiotemporal disparities and highly transmissive characteristics of both DIC and its sources in the K-CZ, which are controlled by multiple factors. This study also highlights that rainfall may play a crucial role in accelerating carbon dynamics in the K-CZ. High-frequency sampling campaigns in high-flow periods and deep analyses are needed in future work to elucidate the related processes and mechanisms. © 2019 John Wiley & Sons, Ltd.

KEYWORDS: dissolved inorganic carbon; carbon isotope; carbonate weathering; spatiotemporal variations; karstic catchment; Southwestern China

Introduction

Carbonate rocks cover ~12% of the Earth's ice-free land area and karst aquifers represent important drinking water reservoirs which provide fresh water for approximately 25% of the Earth's population (Ford and Williams, 2013). It is a key component of the Earth's critical zone (CZ). In a karstic critical zone (K-CZ), the karstic dynamics make the CO_2–H_2O–$CaCO_3$ system susceptible to environmental change (Yuan and Zhang, 2008). Thin soil cover and well-developed conduit networks render the K-CZ catchment highly transmissive, forming large underground drainage systems and resulting in intense fluid–rock interaction and strong carbon dynamics relative to non-karstic conditions. Because of weathering of carbonate minerals, concentrations of dissolved inorganic carbon (DIC) in the CO_2–H_2O–$CaCO_3$ system are approximately 66 times those in the CO_2–H_2O system (Dreybrodt, 1988), and the contribution of biologic carbon to DIC is normally less in karst systems than in non-karst systems. In addition, the large and rapid water fluxes through preferential flow pathways during wet periods can not only shorten the time for transportation and fluid–rock interaction in K-CZ, but also increase the reactive mineral surface area (Clow and Mast, 2010; Zhong *et al.*, 2017b). Therefore, the circulations of carbon (and hydrochemistry) and the DIC dynamics in K-CZ are complex and differ from other non-karstic CZ, bringing related topics to the frontier in the Earth's surface geochemistry (Plummer and Busenberg, 1982; Yuan and Cai, 1988; Schulte *et al.*, 2011; Ford and Williams, 2013; Jiang, 2013; Pu *et al.*, 2017; Song *et al.*, 2017).

The kinetics of carbonate dissolution are more rapid than silicate weathering induced by carbonic acid, which results in a net carbon sequestration into calcites [Equation (1)] (McClanahan *et al.*, 2016). Carbonate weathering offers both a sink and a source of atmospheric carbon. On the one hand, geological sequestration of atmospheric CO_2 and subsequent transformation into DIC, allowing transport by rivers and

eventual deposition in oceans as calcite minerals, is a carbon sink (Regnier *et al.*, 2013). On the other hand, reactions between carbonate minerals and both carbonic acid and other acids can also release CO_2 [Equations (2)–(4)], becoming a source of atmospheric CO_2, despite the fact that CO_2 in Equation (2) acts merely as a proton donor with no overall increase in atmospheric CO_2 (Calmels *et al.*, 2007; Li *et al.*, 2008):

$$CaSiO_3 + CO_2 \rightarrow CaCO_3^{\downarrow} + SiO_2 \quad (1)$$

$$CaCO_3 + H_2O + CO_2 \rightarrow Ca^{2+} + 2HCO_3^- \rightarrow CaCO_3^{\downarrow} + H_2O + CO_2^{\uparrow} \quad (2)$$

$$2CaCO_3 + H_2SO_4 \rightarrow 2Ca^{2+} + 2HCO_3^- + SO_4^{2-} \rightarrow CaCO_3^{\downarrow} + CO_2^{\uparrow} + SO_4^{2-} + Ca^{2+} \quad (3)$$

$$CaCO_3 + 2HNO_3 \rightarrow Ca^{2+} + 2NO_3^- + H_2O + CO_2^{\uparrow} \quad (4)$$

The global consumption of CO_2 by chemical weathering is in the range of 0.22–0.29 Gt C a^{-1}, resulting in approximately 0.4 Gt C a^{-1} of DIC in global rivers, which accounts for approximately 40% of the total riverine carbon flux (Amiotte-Suchet *et al.*, 2003; Lerman *et al.*, 2007; Cai *et al.*, 2008; Hartmann *et al.*, 2009). Therefore, carbonate weathering can not only affect chemical compositions of fluids draining carbonate-dominated terrains, but also regulate biogeochemical circulations of carbon (both on short and long timescales) (Donnini *et al.*, 2016; Zhong *et al.*, 2017a). Similarly, the interaction between carbonate weathering and atmospheric and/or biological CO_2 has potential climatic implications at a regional or even global level (Calabrese *et al.*, 2017; Torres *et al.*, 2017). In turn, based on a global database, the climate also controls the carbonate weathering and thereby exerts influence on the carbon cycle, including the 'boomerang' relationship between carbonate weathering intensity and temperature. Nonetheless, more data in various environmental systems (e.g. small karstic basins) are needed to understand more thoroughly the role that carbonate weathering and overlying ecosystems have played in the Anthropocene (Gaillardet *et al.*, 2018; Zhong *et al.*, 2018).

Stable carbon isotope ratio ($\delta^{13}C$) can be used as a tracer to study weathering and riverine carbon cycles as a result of the isotopic differences between carbonate and biological carbon. Marine carbonate bedrock sources have typical $\delta^{13}C$ of 0‰ (Clark and Fritz, 1997; Shin *et al.*, 2011). The $\delta^{13}C$ of atmospheric CO_2 is currently approximately −8.2‰, which is a decrease from −7.6‰ in the 1980s (Cuntz, 2011). The $\delta^{13}C$ of vegetation depends on specific photosynthetic pathways, commonly including the Calvin Cycle (C3) and the Hatch and Slack Cycle (C4). These pathways induce different amounts of carbon isotope fractionation based on the efficiency of carbon usage, so that C3 and C4 plants can be differentiated by $\delta^{13}C$ of −27‰ (from −24 to −30‰) and −13‰ (from −10 to −16‰), respectively (Vogel, 1993; Clark and Fritz, 1997). The Crassulacean acid metabolism (CAM) photosynthetic pathway is not considered here because its contribution to global net primary productivity is insignificant relative to the C3 and C4 pathways (Marwick *et al.*, 2015). However, there remain many quantification problems and uncertain processes because of joint effects of various complicated factors leading to $\delta^{13}C$ variation and its seasonal patterns, such as the atmosphere–river equilibration of CO_2, photosynthesis and/or respiration, and sampling coverage (partial pressure of CO_2 levels in rivers show large spatial and temporal variations) (Yang *et al.*, 1996; Amiotte-Suchet *et al.*, 1999; Hélie *et al.*, 2002; Wachniew, 2006). All these possible fractionations should be considered when using the isotope approach to identify carbon sources and cycling; current constraints are insufficient and need to be settled with comprehensive future research.

Although a growing number of researches have employed water chemistry and $\delta^{13}C$ to constrain carbon sources and related controls in aquatic systems, most studies have focused on large river basins or non-karstic watersheds, and limited research has highlighted the carbon characteristics in the K-CZ of small basins with monthly samples. However, because of those characteristics of K-CZ (e.g. high permeability and carbonate dissolution), the contribution ratios of DIC sources here are more variable and the spatiotemporal patterns are also different from the non-karstic basin. Again, small-scale studies involve manageable data sets and can provide detailed data on particular regions, within a given climate, necessary for synthesis into large-scale compilations. Against that background, the Houzhai basin, a 73.4 km^2 karstic catchment, was selected as the research area to analyse monthly dissolved solutes and DIC characteristics, in order to: (1) depict the spatiotemporal variations of DIC in the K-CZ catchment; (2) partition the possible sources of DIC using isotopes and the mixing model IsoSource; (3) elucidate dominant controlling factors; and (4) explore the optimal time needed to conduct high-frequency sampling campaigns for observing DIC dynamics. The ultimate purpose is to provide fundamental data for modelling carbon dynamics in the K-CZ catchment and to reveal water–carbon coupling mechanisms as well as controls of relevant biogeochemical processes.

Materials and methods

Study area and sampling sites

The Houzhai catchment (26°13′3″–26°15′3″N, 105°41′27″–105°43′28″E) is located in Puding County, Guizhou Province, Southwestern China, which is in the centre of the Southeast Asian Karst Region, which is the largest continuous karst area in the world (Dianwu and Seip, 1991; Li *et al.*, 2010).

The catchment is controlled by a sub-humid monsoon climate, dry and cold during winter, wet and warm during summer, with an average annual temperature and rainfall of 20.1°C and 1300 mm, respectively. It is on the dividing zone between the Yangtze River Basin and the Pearl River Basin. Its altitude ranges from 1218 to 1565 m a.s.l. (outlet elevation of 1250 m), declining from the southeast to the northwest. The area shows a pattern of landscape evolution from peak-clumped depressions to trough valleys to peak forests with plains (Zhang *et al.*, 2017).

The lithology of this catchment is primarily middle Triassic carbonates, with abundant but minor clastic sedimentary rocks and minor strata of interbedded gypsum (Chen *et al.*, 2008; Li *et al.*, 2010). The Houzhai catchment covers 73.4 km^2, of which 51.0% is arable land, followed by forest (32.8%) and built land (12.1%). In this catchment, soils are thin (<40 cm) and continuously distributed in hills, and only some valleys in the upstream have soils deeper than 100 cm. The agricultural land is, therefore, primarily located in the middle and lower reaches of the catchment.

Sampling sites in the Houzhai catchment (Figure 1) were classified into three types: underground water (UGW, including No. 1 to No. 5 in the upper reaches, No. 6 and No. 7 in the middle reaches, No. 10 in the lower reaches); surface streams (SFS, No. 8 in the outlet of the Qingshan reservoir and No. 9 in the outlet of the surface river); and water from the total outlet

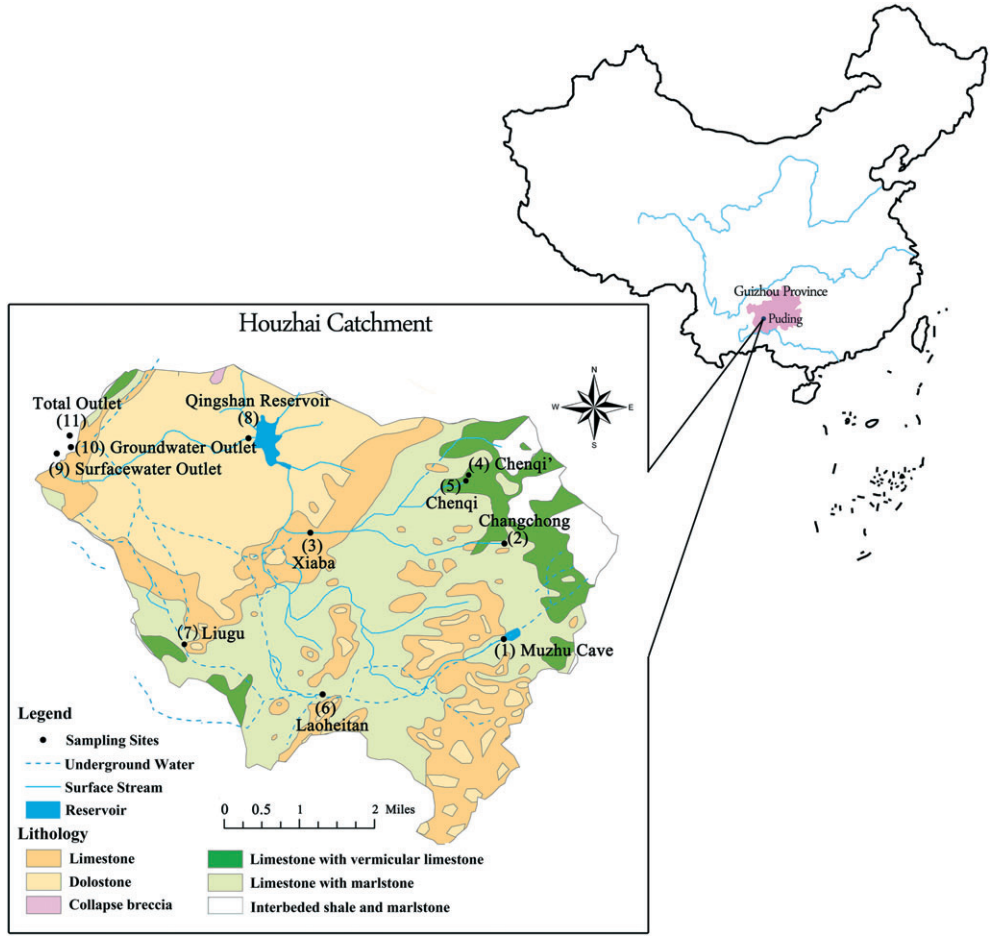

Figure 1. Location of the study area and sampling sites. This figure shows our research area – Houzhai catchment in Puding County, Guizhou Province in Southwestern China and 11 sampling sites in the Houzhai catchment – together with lithologic character distribution. [Colour figure can be viewed at wileyonlinelibrary.com]

of this catchment (TOW, i.e. No. 11) after convergence of the outlets of Nos 9 and 10 (the outlet of underground water). The mean annual discharges of Nos 9 and 10 are 24.9×10^6 and 23.3×10^6 m^3, respectively, and together account for more than 95% of the total discharge of the whole catchment. In addition, the water flow during the wet season (from May to October) comprises approximately 99 and 68% of the respective annual amount at Nos 9 and 10 (Chen *et al.*, 2005).

Sample collection and analysis methods

Samples were collected on a monthly basis from January to December 2013 (around the 21st of each month) at 11 sites (Figure 1). An additional field campaign was conducted on 9 June 2013 when there was a daily rainfall of 55.8 mm. In all, 162 samples were collected for hydrochemical and DIC analysis. It is worth highlighting that site No. 4 is at the outlet of a new spring formed during a drilling test, possibly in 2011. This spring has relatively stable discharge and hydrological characteristics, and is believed to have been impacted by interbedded gypsum strata distributed under the thin marlstone layer distributed between the Chenqi and Changchong sites (Figure 1).

A portable multi-parameter meter was applied to detect water quality at every sampling site, including water temperature (T), dissolved oxygen (DO), pH and electrical conductivity (EC). Triplicate water samples were collected in polyethylene bottles, which were all cleaned with autochthonous water beforehand, in order to analyse alkalinity, major ions and dissolved organic carbon (DOC). All samples were immediately stored in darkness at 4°C for future treatment.

Bicarbonate contents were determined promptly by the standard acid titration method with 0.02 mol l^{-1} HCl. Samples for the measurement of main ions were filtered through membrane microfilters (0.22 μm, Millipore) with injectors firstly and then were further separated into two parts; one was acidified to pH < 2 with ultra-purified nitric acid (preventing complexation and precipitation) to measure major cations (Na^+, K^+, Ca^{2+}, Mg^{2+}) using inductively coupled plasma optical emission spectrometry (ICP-OES) and the other non-acidified filtrate was used to determine the main anions (SO_4^{2-}, Cl^-, NO_3^-) by Dionex ion chromatography systems 90 (ICS 90). The standard errors of these methods were both better than 5%. In addition, DOC contents were detected as CO_2 using catalytic combustion, similar to the method described by Li *et al.* (2010).

For stable isotopic compositions of DIC, samples were collected and prepared using a method modified from Atekwana and Krishnamurthy (1998), and the specific steps were the same as previously reported (Zhong *et al.*, 2017b). $^{13}C/^{12}C$ (R) was measured by mass spectrometer (MAT 252, Finnigan) in the State Key Laboratory of Environmental Geochemistry, Guiyang, China. The measurement precision is better than 0.2‰ and the final data were reported using delta (δ) notation relative to the Vienna Pee Dee Belemnite (V-PDB) in per mil (‰) as follows:

$$\delta^{13}C\ (‰) = \left(R_{sample}/R_{standard} - 1\right) \times 10^3 \qquad (5)$$

Finally, the partial pressure of carbon dioxide (pCO_2) in water, the saturation state index of calcite (SIc) and DIC

concentrations were computed based on mass action relationships, relative equilibrium constants and thermodynamic constants (Plummer and Busenberg, 1982; Clark and Fritz, 1997).

Results

Water quality and hydrochemical characteristics

The T, pH, EC and DO in the Houzhai catchment in 2013 were in the range of 6.8–29.3°C (mean 18.4°C), 7.0–9.2 (mean 7.6), 235–2090 μS cm^{-1} (mean 783 μS cm^{-1}) and 0.7–11.9 mg l^{-1} (mean 6.0 mg l^{-1}), respectively. All sites (except site No. 4) had significant seasonal variations of T, pH, EC and DO (and water discharge).

The concentrations of total dissolved solids (TDS = $[Ca^{2+}]$ + $[Mg^{2+}]$ + $[Na^{+}]$ + $[K^{+}]$ + $[SO_4^{2-}]$ + $[HCO_3^{-}]$ + $[Cl^{-}]$ + $[NO_3^{-}]$) varied seasonally, from 267.9 to 1268.9 mg l^{-1}, with an annual mean of 577.7 mg l^{-1}. Site No. 4 had the largest TDS (mean 1192.1 mg l^{-1}), but with minor variations (Figure 2a). TDS at the other sites had an obvious seasonal variation in descending order of spring, winter, autumn and summer, and were bigger in the dry season (October–March) than in the wet season (April–September). Spatially, TDS in UGW were generally higher than in SFW, and values of the coefficient of variation (CV) also indicated that TDS fluctuated more widely in UGW than in SFS.

The hydrochemistry of this study presented different ion ratios in detail when compared with other publications, although their general trends were partially similar (Figure 3). Ca^{2+} and Mg^{2+} dominated the cations within the range of 1.05–6.61 and 0.45–2.41 mmol l^{-1} (mean 2.63 and 1.16 mmol l^{-1}), respectively; their sum accounted for 89.4% of cations (61.6% for Ca^{2+} and 27.8% for Mg^{2+}). The contents of Na^{+} and K^{+} were typically much lower, with mean values of 0.34 and 0.08 mmol l^{-1}, respectively. HCO_3^{-} was the principal anion, accounting for 65.2% (from 37.2 to 86.3%). The second major constituent was SO_4^{2-} and a proportion of 24.8% (from 7.6 to 62.4%), while proportions of NO_3^{-} (mean 5.6%) and Cl^{-} (mean 4.4%) were relatively low. The concentrations of these anions were in the range of 2.42–5.38, 0.30–6.87, null–1.03 and 0.02–0.66 mmol l^{-1} (mean 3.88, 1.76, 0.31 and 0.25 mmol l^{-1}), respectively.

The temporal changes of Ca^{2+}, Mg^{2+} and SO_4^{2-} were approximately the same as those of TDS, while the variations of NO_3^{-} were distinctive, with elevated concentrations generally occurring in the wet season apart from sites No. 4 and 6. There were no clear distinct seasonal differences for diverse sampling sites in HCO_3^{-} content. Of the 11 sites, No. 4 showed the highest annual average concentrations of Ca^{2+}, Mg^{2+} and SO_4^{2-}, but the NO_3^{-} concentrations here were very low and even below the detection limit. It is also worth noting that every ion concentration at TOW was closely matched by that at No. 10; their standard deviation (SD) was less than or close to 5.0% except for HCO_3^{-} (7.3%) for all annual mean ion concentrations.

Dissolved carbon characteristics

DOC contents fluctuated from 0.10 to 10.48 mg l^{-1} with an average value of 1.58 mg l^{-1}; most were less than 2 mg l^{-1} and only 6.8% of 162 samples exceeded 4 mg l^{-1}, including two outliers (10.48 mg l^{-1} at site No. 8 in April and 9.97 mg l^{-1} in one headwater sample on 9 June), which might have been contaminated by incoming sanitary sewage. Figure 2b shows that SFS had higher DOC contents than UGW. For SFS, the average DOC concentrations were higher in the dry season than in the wet season, whereas UGW showed a reversed seasonal pattern.

Among DIC species, HCO_3^{-} was the dominant component and accounted for 93.9% (from 82.7 to 98.3%). DIC concentrations ranged from 2.52 to 5.85 mmol l^{-1} (mean 4.15 mmol l^{-1})

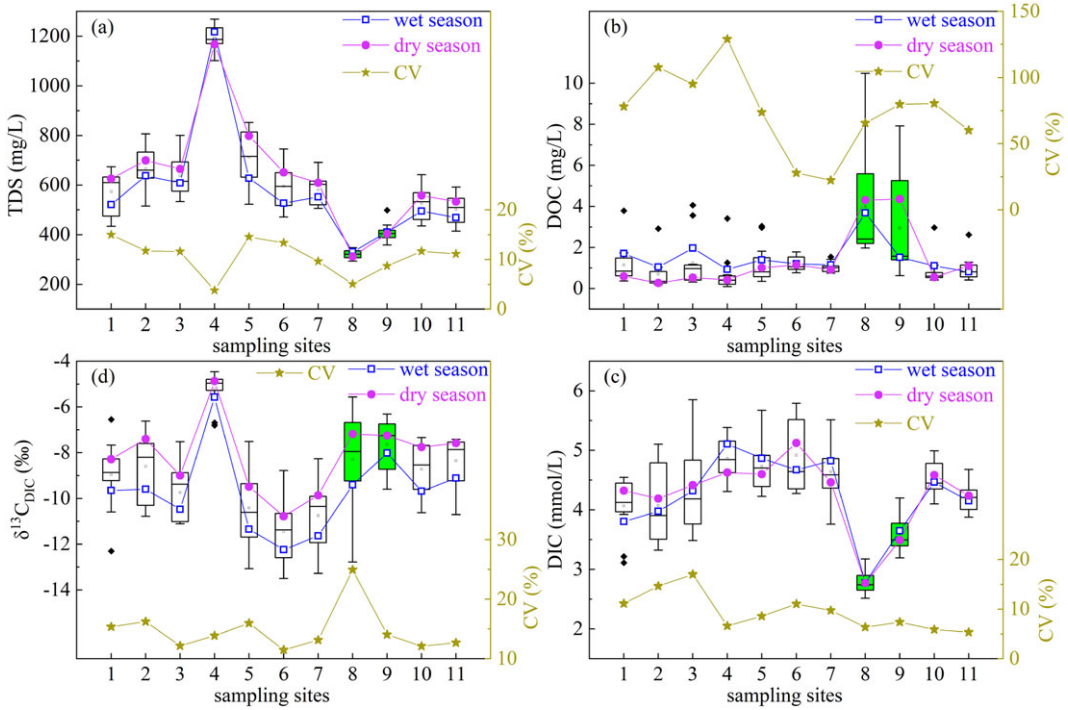

Figure 2. Seasonal differences and ranges of some parameters in water samples changing from the upper stream to the lower reaches of the Houzhai catchment. The green box plots (Nos 8 and 9) refer to surface water. CV (%) refers to the coefficients of variation, reflecting the dispersion degree of parameters. This figure indicates that TDS, DOC, DIC and $\delta^{13}C_{DIC}$ all present spatiotemporal variations, and have different fluctuations reflected by their CV values, demonstrating that water flow path/types can influence these parameters to some extent. [Colour figure can be viewed at wileyonlinelibrary.com]

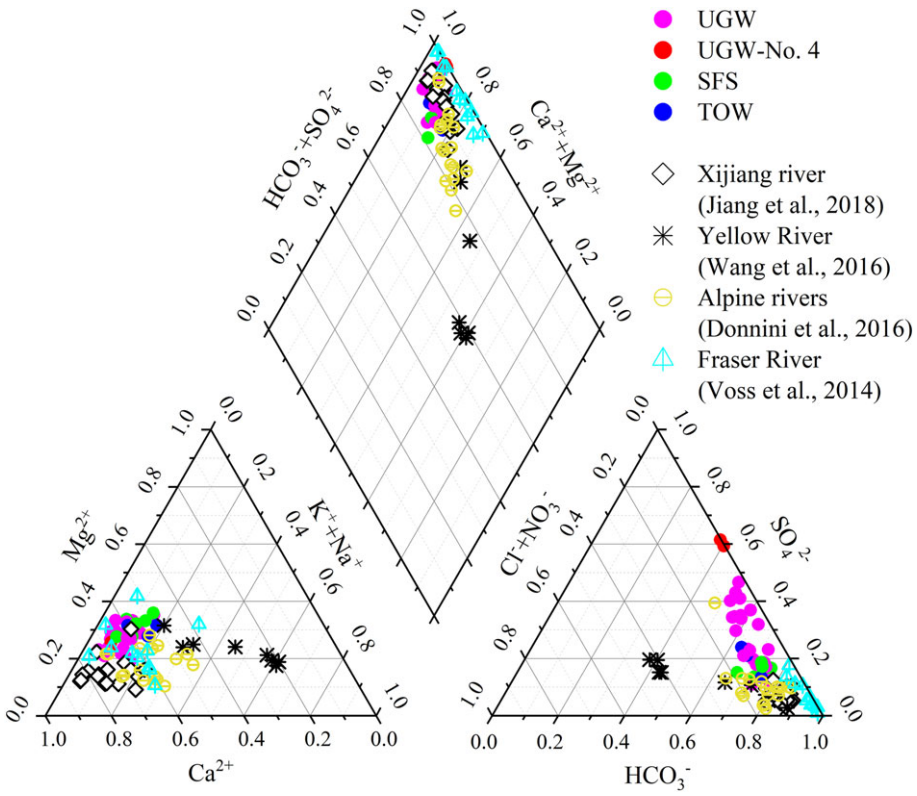

Figure 3. Piper diagram showing ion compositions in the Houzhai catchment for this study. The figure shows the compositions of major anions and cations, together with results from other publications about karstic and non-karstic areas, for comparison and to find the differences in hydrochemistry of different research areas. Ca^{2+} and Mg^{2+} dominate the cations, HCO_3^- and SO_4^{2-} are the principal anions. The hydrochemistry of this study presents different ion ratios in detail when compared with other publications, although their general trends are partially similar. [Colour figure can be viewed at wileyonlinelibrary.com]

and were higher in UGW than in SFS (Figure 2c). Unlike DOC and TDS, DIC had complex seasonal patterns at different sites but relatively minor temporal fluctuations (reflected by CV), especially in the middle and lower reaches (Figure 2).

SIc was in the range of −0.33 to 1.91 (mean 0.44), and more than 90% of samples had SIc > 0. Mostly, UGW had lower SIc values than SFS. In addition, UGW exhibited lower SIc in the wet season than in the dry season, except at site No. 4, whose seasonal trend did the opposite and was in accord with two other SFS sites.

pCO_2 in water varied from $10^{-3.9}$ to $10^{-1.7}$ (atm) with a mean of $10^{-2.2}$ (atm) and was lower in only five samples (four from site No. 8 and one from site No. 9) than in the atmosphere ($10^{-3.5}$ atm). Contrary to spatiotemporal distributions of SIc, pCO_2 was higher in UGW than in SFS, and all sites (except No. 8) tended to generate larger pCO_2 in the wet season than in the dry season. In addition, the minimum CV of pCO_2 occurred at site No. 4.

$\delta^{13}C_{DIC}$ values ranged from −15.7 to −4.5‰ (mean −9.6‰), with CV of 26.0% (n = 162) (Figure 2d). The average $\delta^{13}C_{DIC}$ value of the whole Houzhai catchment was more negative in the wet season than in the dry season (−9.7‰ vs −8.1‰), and every site followed this seasonal pattern. Of all the sites, No. 4 had the biggest annual mean $\delta^{13}C_{DIC}$ (−5.2‰) and the lowest CV. After excluding site No. 4, UGW showed more depleted $\delta^{13}C$ values than SFS.

Discussion

Spatiotemporal variations of dissolved solutes

In this study, TZ^+ (the total charge of dissolved cations) ranged from 3.6 to 18.4 mEq l^{-1} (mean 8.0 mEq l^{-1}), which was not only higher than most large rivers in China [e.g. mean 3.0 mEq l^{-1} for Xijiang River (Jiang *et al.*, 2018) and 4.1 mEq l^{-1} for the Wujiang and Yuanjiang River draining karst terrain (Han and Liu, 2004)], but also surpassed the average values in other areas [e.g. 3.5 mEq l^{-1} for Alpine rivers (Donnini *et al.*, 2016) and 1.2 mEq l^{-1} for the Fraser River (Voss *et al.*, 2014)], revealing the intensive rock weathering in the Houzhai basin. The relationship between TZ^+ and TZ^- (the total charge of dissolved anions) yielded a highly significant correlation coefficient (R^2) of 0.97 (n = 162), and the net inorganic charge balance [NICB = $(TZ^+ - TZ^-) * 100/ (TZ^+ + TZ^-)$] of almost all samples was within ±5, implying that all considered cations and anions were in mutual equilibrium and the contribution of unanalysed organic anions was negligible.

The equivalent ratios of $(HCO_3^- + SO_4^{2-})$ to $(Ca^{2+} + Mg^{2+})$ in all samples were close to a constant value of 1 and, as shown in Figure 4, the molar ratios of $[Ca^{2+} + Mg^{2+}] / [HCO_3^-]$ were mostly within 0.5 and 1.0 (excluding site No. 4), indicating that carbonate weathering by carbonic acid was the primary mode and other acids might also have taken part in the reaction restrained by $\delta^{13}C_{DIC}$ and the stoichiometry of Equations (2)–(4). The high values of $[Ca^{2+} + Mg^{2+}] / [HCO_3^-]$ at site No. 4 (mean 1.9) suggest that hydrochemistry here was impacted by gypsum dissolution because of the minor strata of interbedded gypsum in this catchment (Li *et al.*, 2010). Site No. 4 belongs to deep confined water draining a gypsum horizon with little anthropogenic inputs, resulting in minimal $[NO_3^-]$ and lower CV values for most ions and lower TDS compared with corresponding parameters at other sites. As shown in Figure 5, the application of fertilizer or/and manure as well as biogenic CO_2, which is a by-product of microbial respiration, can influence carbon isotopic signals to some extent. In the karstic region of Southwestern China, the thin soils and vadose zone with weak buffering

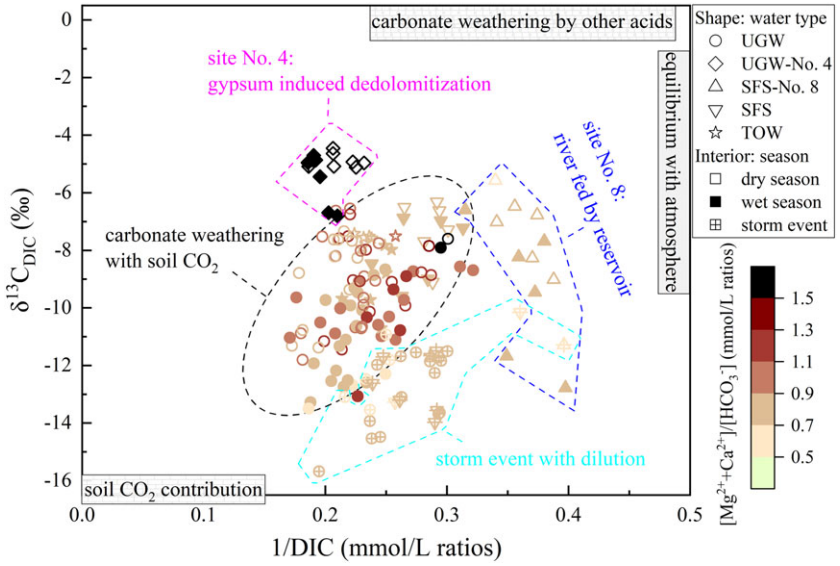

Figure 4. Scatter plot showing the relationship between $\delta^{13}C_{DIC}$ (‰), the reciprocal of DIC (mmol l^{-1}) concentrations and the molar ratios of [Ca^{2+} + Mg^{2+}] / [HCO_3^-]. This figure indicates that carbonate weathering by carbonic acid is the primary mode and other acids may also take part in the reaction. Site No. 4 is significantly influenced by gypsum-induced dedolomitization. Soil CO_2 is the primary contributor to DIC in most groundwater, while atmospheric CO_2 may be another riverine DIC source for surface water which can be influenced by the uptake of carbon by photosynthesis. Rainstorms can also affect DIC sources and $\delta^{13}C_{DIC}$. [Colour figure can be viewed at wileyonlinelibrary.com]

enable contaminants, such as NO_3^-, to migrate quickly within the surface–underground system (Chen *et al.*, 2008; Perrin *et al.*, 2008). This may be responsible for the observation that NO_3^- concentrations in UGW were higher than those in SFS, which is inconsistent with results in non-karstic areas (Li *et al.*, 2013). In addition, the large fluctuation of NO_3^- concentrations through time mainly relates to the periodicity of agricultural activities. Nitrogen loading in the Houzhai catchment was mainly derived from manure and reductive nitrogen fertilizer, and NO_3^- here presented nitrification characteristics (Yue *et al.*, 2018), which have been proven to promote soil degradation and carbonate weathering in the intensively cultivated Garonne basin (Semhi *et al.*, 2000). Degradation of organic matter in soil will generate biogenic CO_2 and organic acids,

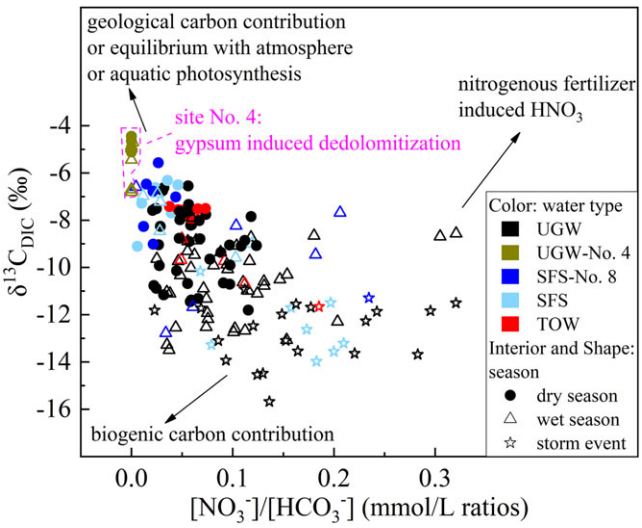

Figure 5. Scatter plot showing the relationship between $\delta^{13}C_{DIC}$ and ratios of [NO_3^-] to [HCO_3^-] in water samples. This figure shows some controlling factors and processes for $\delta^{13}C_{DIC}$ (e.g. gypsum-induced dedolomitization, CO_2 equilibrium with atmosphere, aquatic photosynthesis and nitrogenous fertilizer usage, especially during farming periods in the wet season). [Colour figure can be viewed at wileyonlinelibrary.com]

both of which are beneficial to carbonate dissolution; the former can enrich ^{12}C in DIC, but the effect of the latter may be insignificant because of limited water–rock interaction in running water, especially during the wet season. In addition, when denitrifying bacteria utilize organic carbide as the carbon source to trigger denitrification, the simultaneous product of biogenic CO_2 can also alter the $\delta^{13}C_{DIC}$ towards more negative values. In this catchment, denitrification happens primarily in the wet season under circumstances of heavy rain and high temperatures (Yue *et al.*, 2015).

Compared with 2007 (Li *et al.*, 2010), the annual mean contents of ions were higher but the seasonal variations of DIC were minor in 2013 (this study), which may be a result of less rainfall in 2013 (total of 732 mm, with 79.4% in the wet season) than in 2007 (total of 1274 mm, with 87.1% in the wet season). The distinct lower amount of rain in 2013 generated a weaker dilution effect, which might impact ion concentrations to some extent but would not significantly affect DIC or be disguised by the seasonal variation of DIC sources. The attendant restricted soil water would tend to restrict plant growth rates and bioactivity in soil, thus promoting the diffusion of soil CO_2 to the atmosphere (Ilstedt *et al.*, 2000; Romero-Mujalli *et al.*, 2018). In addition, the sampling sites in 2007 did not include site No. 4 draining from a deep gypsum layer with the highest concentrations of TDS and DIC. Furthermore, bi-annual sampling in April and July 2007, relative to more frequent monthly collections in 2013, might not fully represent variations between the dry and wet seasons.

Table I presents an overview of seasonal variations in 2007 and 2013 for some parameters at three outlets. Clearly, these parameter values at the total outlet (No. 11) were between UGW and SFS and almost all were closer to site No. 10 than to site No. 9 in both years. It is likely that the water flux at site No. 11 was mostly contributed to by site No. 10 (Yue *et al.*, 2018). During high-flow months, continual rainfall can boost the exchange between surface–underground systems through wells, sinkholes and karst aquifer networks, and overland runoff can enhance the contribution proportion of surface water to the basin outlet (Zhang *et al.*, 2017), finally reducing the differences in many parameters among the three outlets. However, the dry season features lower amounts of rain and

Table I. Average annual, wet season and dry season values of some major parameters at the outlet of the surface water (No. 9), underground water (No. 10) and total vent (No. 11) in the Houzhai basin in 2013 and 2007 (Li et al., 2010)

	TDS (mg l^{-1})			DOC (mg l^{-1})			DIC (mmol l^{-1})			SIc			pCO_2 (atm) in water			$\delta^{13}C_{DIC}$ (‰)		
	No. 9	No. 10	No. 11	No. 9	No. 10	No. 11	No. 9	No. 10	No. 11	No. 9	No. 10	No. 11	No. 9	No. 10	No. 11	No. 9	No. 10	No. 11
2013 annual	407	527	501	2.94	0.83	0.96	3.57	4.53	4.20	0.86	0.17	0.47	$10^{-2.8}$	$10^{-2.1}$	$10^{-2.4}$	−7.6	−8.7	−8.4
Wet season	411	495	469	1.52	1.11	0.81	3.65	4.47	4.15	0.87	0.15	0.33	$10^{-2.6}$	$10^{-2.0}$	$10^{-2.2}$	−8.0	−9.7	−9.1
Dry season	404	558	534	4.36	0.56	1.10	3.49	4.58	4.24	0.84	0.18	0.60	$10^{-3.0}$	$10^{-2.1}$	$10^{-2.6}$	−7.3	−7.8	−7.6
2007 annual	389	462	458	2.65	1.10	1.54	3.76	4.00	3.95	0.70	0.29	0.47	$10^{-2.8}$	$10^{-2.3}$	$10^{-2.5}$	−8.2	−8.9	−8.4
Wet season	381	405	405	1.68	0.85	1.23	3.42	3.88	3.80	0.85	0.27	0.48	$10^{-2.9}$	$10^{-2.3}$	$10^{-2.5}$	−9.1	−10.2	−9.4
Dry season	397	519	511	3.62	1.35	1.85	4.10	4.12	4.11	0.55	0.32	0.45	$10^{-3.7}$	$10^{-2.4}$	$10^{-2.5}$	−7.2	−7.6	−7.4

longer hydraulic retention time, coupled with the effect of evaporation, resulting in heavier $\delta^{13}C_{DIC}$ than in the wet season, especially for surface water under open conditions.

The lower DIC contents in SFS relative to UGW might be ascribed to DIC consumption by secondary $CaCO_3$ formation and losses by CO_2 degassing to the atmosphere [inverse reaction of Equation (2)]. This is supported by higher SIc and lower pCO_2 in SFS than in UGW.

Besides, two good relationships between DIC, SIc and pCO_2 in water were found based on data from 2007 and 2013 [i.e. DIC = log pCO_2/0.44 + 9.68 (R^2 = 0.5) and log pCO_2 = −SIc/0.70 + 1.81 (R^2 = 0.8)], indicating that the DIC contents were also related to internal equilibration between different carbonate species. Based on the two functions, it is possible to infer that, when DIC is below 1.73 mmol l^{-1}, there is a tendency to cause calcite precipitation, and atmospheric CO_2 possibly provides inorganic carbon to water, while when DIC is in the range of 1.73–5.57 mmol l^{-1}, calcite as well as CO_2 in water are both oversaturated, perhaps generating calcite precipitation and CO_2 release to the ambient atmosphere. In addition, it can also be observed in Figure 6 that there is a strong positive relationship between TDS concentrations and log pCO_2, denoting that a higher pCO_2 level in water can promote dissolution. The increase of pCO_2, as well as the dilution of TDS, might explain the poorer correlation during the wet season compared with the dry season.

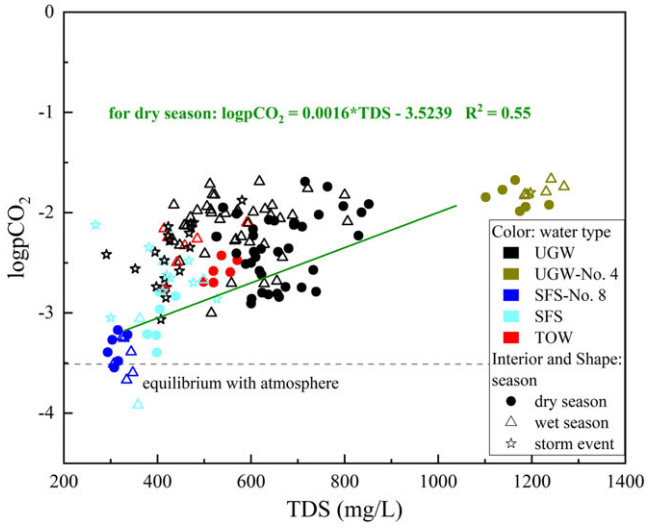

Figure 6. Scatter plot showing the relationship between log pCO_2 and TDS in water samples. This figure indicates that there is a strong positive relationship between TDS concentrations and log pCO_2, denoting the fact that a higher pCO_2 level in water can promote dissolution, especially in the dry season. [Colour figure can be viewed at wileyonlinelibrary.com]

Carbon isotopic evolution

In natural groundwater, the DIC sources are (1) the dissolution of soil CO_2 derived from root respiration and the decay of labile soil organic matter in the soil zone and (2) carbonate weathering. For surface water, such as rivers and lakes/reservoirs, the biogenic CO_2 produced during organic matter degradation may also be a significant contributor to DIC in water with a high nutrient level (Clark and Fritz, 1997). The average $\delta^{13}C$ of soil organic carbon ($\delta^{13}C_{soc}$) in Puding County is −21.2‰ for profiles of limestone yellow soil and −23.3‰ for profiles of sandstone yellow soil (Tian *et al.*, 2013). Using their mean (−22.3‰) to represent $\delta^{13}C_{soc}$, the $\delta^{13}C$ of soil CO_2 in this region is approximately −18‰ after taking into account an isotopic enrichment of +4.4‰ caused by molecular diffusion (Cerling *et al.*, 1991), resulting in DIC with $\delta^{13}C$ value of −18‰. The dissolved CO_2 weathers aquifer carbonates of marine origin with a $\delta^{13}C$ value of ~0‰ (Clark and Fritz, 1997).

There was a positive relationship between the reciprocal of DIC and $\delta^{13}C_{DIC}$ for UGW (omitting site No. 4, Figure 4), indicating that the DIC can be explained by two mixtures of soil CO_2 and carbonate weathering. Both the elevated values of $\delta^{13}C_{DIC}$ and DIC at site No. 4 might be caused by gypsum-induced dedolomitization (Appelo and Postma, 2005). During this process, the $\delta^{13}C_{DIC}$ of groundwater may increase beyond the initial signal of soil CO_2 and carbonate with increasing residence time. Although the involvement of exogenic acids (i.e. H_2SO_4 and/or HNO_3) in carbonate weathering will also increase $\delta^{13}C_{DIC}$ values, it is less likely to be the case at site No. 4, since (1) there is no geological evidence for the exposure of pyrite in this catchment and (2) the spring contains only a tiny amount of NO_3^-. However, for the rest of the sampling sites, the carbonate dissolution by H_2SO_4 (from acid deposition) and/or HNO_3 (produced by chemical fertilizer application) may be a potential factor, considering the stoichiometric relationship between $\delta^{13}C_{DIC}$ and $[NO_3^-]/[HCO_3^-]$ ratios (Figure 5).

The relatively higher value of $\delta^{13}C_{DIC}$ in SFS may be partially attributed to CO_2 exchange between the water–atmosphere boundary (Amiotte-Suchet *et al.*, 1999), which can also be deduced from low pCO_2 and high SIc in SFS. In addition, photosynthesis can fix CO_2 to organic carbon by preferentially incorporating ^{12}C, hence increasing both the DOC concentrations and the $\delta^{13}C_{DIC}$ values (Clark and Fritz, 1997). This is demonstrated in Figure 7, which shows that DIC concentrations decreased with an increase in DOC concentrations and $\delta^{13}C_{DIC}$ values. Site No. 8 (fed by the reservoir) had the highest DOC and the lowest DIC concentrations, and $\delta^{13}C_{DIC}$ were also more positive at site No. 8 than at other sites (except No. 4). These provide strong evidence that the lighter carbon in DIC was consumed by aquatic photosynthesis, and in turn produced more DOC, which was similar to the study of some reservoirs in the karst region of Southwestern China (Yu *et al.*, 2008).

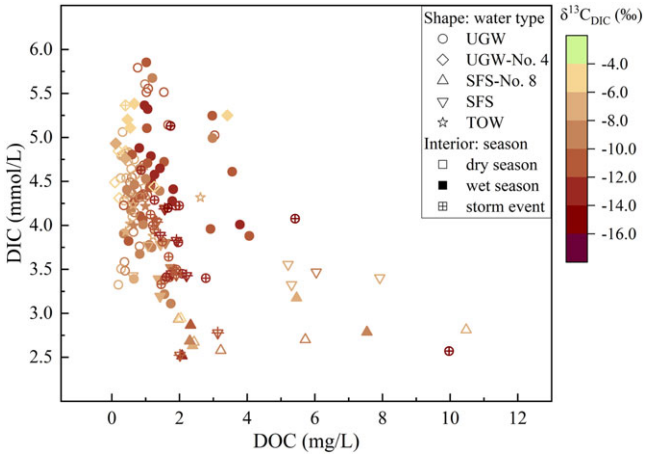

Figure 7. Scatter plot showing the relationship between DIC and DOC concentrations along with the colour code of $\delta^{13}C_{DIC}$. This figure shows the relationship between DIC and DOC concentrations, indicating that DIC concentrations decreased with increasing DOC concentrations and $\delta^{13}C_{DIC}$ values; there are multiple factors leading to mutual transformation of DIC and DOC, then altering the $\delta^{13}C_{DIC}$ values. [Colour figure can be viewed at wileyonlinelibrary.com]

Dynamics of DIC sources

In most karstic aquifer networks, particularly the underground conduits, it is difficult for sufficient atmospheric CO_2 to enter the water because of the lower pH (<5.6) (Wu *et al.*, 2012) in rainfall and the higher pCO_2 in water (>$10^{-3.5}$ atm) (Li *et al.*, 2010; McClanahan *et al.*, 2016). In this study, the higher pCO_2 in underground water (>$10^{-3.5}$ atm) indicates that the atmospheric contribution to DIC can be ignored in UGW. But the two SFS showed some lower pCO_2 (<$10^{-3.5}$ atm), so the atmospheric CO_2 was likely to be one DIC source in these open systems and should be considered when calculating their contributions, even though their contribution ratio may be low.

In order to deduce possible contributions of DIC sources to water mixtures over temporal scales in the Houzhai catchment, the IsoSource (v1.3) programme was employed with an increment of 1.0% and a mass balance tolerance of 0.5‰ based on carbon isotope signals from various sources.

As previously established, −18‰ can be used as the isotopic signal of DIC which originates from soil CO_2 or subsequent reaction with silicates considering the nearly closed system, being denoted as Source 1. The $\delta^{13}C$ of DIC generated from the dissolution of carbonates by soil CO_2 was thus assumed to be −9‰ (Source 2). Sulfuric acid (produced by pyrite oxidation or acid rain in Southwestern China) (Li *et al.*, 2008; Jiang, 2013) and nitric acid (produced by chemical fertilizer usage in this agricultural catchment) can also interact with carbonate rocks and shift $\delta^{13}C_{DIC}$ towards 0‰ (Source 3). In addition, the influx of atmospheric CO_2 was assumed as another riverine DIC source but only for the two SFS sites, namely Source 4, whose model input for $\delta^{13}C_{DIC}$ depended on the temperature given the equilibrium fractionation between atmospheric CO_2 and riverine DIC in the open system, enriching the ^{13}C by $\epsilon_{HCO3\text{-}gas} = -(0.141 \pm 0.003) * T\,(°C) + (10.78 \pm 0.05)$‰ when HCO_3^- is the predominant component among DIC species (Zhang *et al.*, 1995).

The results of the IsoSource are presented in Figure 8. It is apparent that DIC in most underground water mainly came from soil CO_2 or/and its reaction with carbonate, except for site No. 4, where DIC was impacted by gypsum-induced dedolomitization. The respective contribution of different sources to DIC shows a wider fluctuation in high-flow months than in low-flow months (Figure 8), demonstrating that meteorological factors in the wet season could affect the DIC sources in karstic water (Calmels *et al.*, 2014). Higher rainfall and temperature during the wet season can encourage microbial activities and hence boost the generation of biogenic carbon, leading to the mutual transformation of DIC and DOC, which altered the $\delta^{13}C_{DIC}$ values (Figure 7).

In order to pinpoint the spatiotemporal variation of DIC sources more clearly, they were classified further into three original end-members (Table II), namely $CaCO_3$, soil CO_2 and atmospheric CO_2, based on data generated from the IsoSource program and stoichiometry. The results show that the relative contribution ratios of these end-members at each site varied both spatially and temporally. During the wet season, soil CO_2 was the primary contributor to DIC in both UGW and SFS. The only exception was site No. 4, where $CaCO_3$ was the dominant source of DIC during the whole hydrologic year. During the dry season, soil CO_2 was the dominant contributor to DIC in UGW in the middle reaches (sites No. 5–7), while the contribution ratios of the carbonate source were bigger than those of soil CO_2 at the rest of the UGW sites. In addition to soil CO_2 and $CaCO_3$, atmospheric CO_2 also contributed to DIC in SFS (sites No. 8 and 9), accounting for 17.7–21.6%.

Similar to the results of hydrochemistry and DIC content, site No. 4 had relatively constant sources of DIC, dominated by $CaCO_3$ which accounted for 69.0 and 72.8% in the wet and dry season, respectively (Table II). This conclusion further demonstrated that gypsum-induced dedolomitization might impact DIC content at this site.

For all sampling sites, contribution ratios of soil CO_2 were higher in the wet season than in the dry season (Table II). This finding might be ascribed to: (1) the greater bio-production as a result of higher temperatures in the wet season than in the dry season (21.5 vs 11.7°C during the sampling period); (2) more rainfall in the wet season, which can bring soil CO_2 into fluid; and (3) the change of dominant flow. Soil moisture and temperature are two factors which affect soil CO_2, both in terms of diffusion to ambient air and dissolution in soil pore water (Gaillardet *et al.*, 2018). Low soil moisture can not only benefit the diffusion of soil CO_2 to the atmosphere, but also limit the growth rate of plants and then organism activities in soil (Ilstedt *et al.*, 2000). The research region is profoundly influenced by a subtropical monsoon climate, leading to abundant moisture and elevated temperatures in the wet season, which could facilitate increased soil organic activity and plant respiration, generating ^{12}C-enriched soil CO_2. Again, dominant flow is likely to change under different hydrological conditions (Bowes *et al.*, 2005), possibly from slow base flow (through tiny fissures/matrix) during the low-flow season to quick flow (through large fractures/conduits) during the high-flow season after saturating the epikarst aquifer. Hydrological conditions are relatively stable during the low-flow season and hence result in steady DIC sources which come mainly from lateral fluid. While the high-flow season can induce wide hydrological changes, soil CO_2 produced by vibrant organisms and soil respiration tends to subsequently be transported by fast infiltration processes to underground conduits without enough time to have contact with rocks, thereby increasing the contribution of soil CO_2 to DIC (Cai *et al.*, 2015; Gaillardet *et al.*, 2018). In addition, the production of soil CO_2 is one of the dominant factors controlling carbonate weathering intensity at a regional scale (Yang *et al.*, 2012; Calmels *et al.*, 2014). While all available monthly data in this study can be used to prove the existence of the influence of soil moisture and temperature in the seasonal variations of DIC sources, especially in the contribution of soil CO_2, it is not enough to capture the range of dynamics needed to describe detailed processes and estimate parameter loads, because of the lack of high temporal resolution

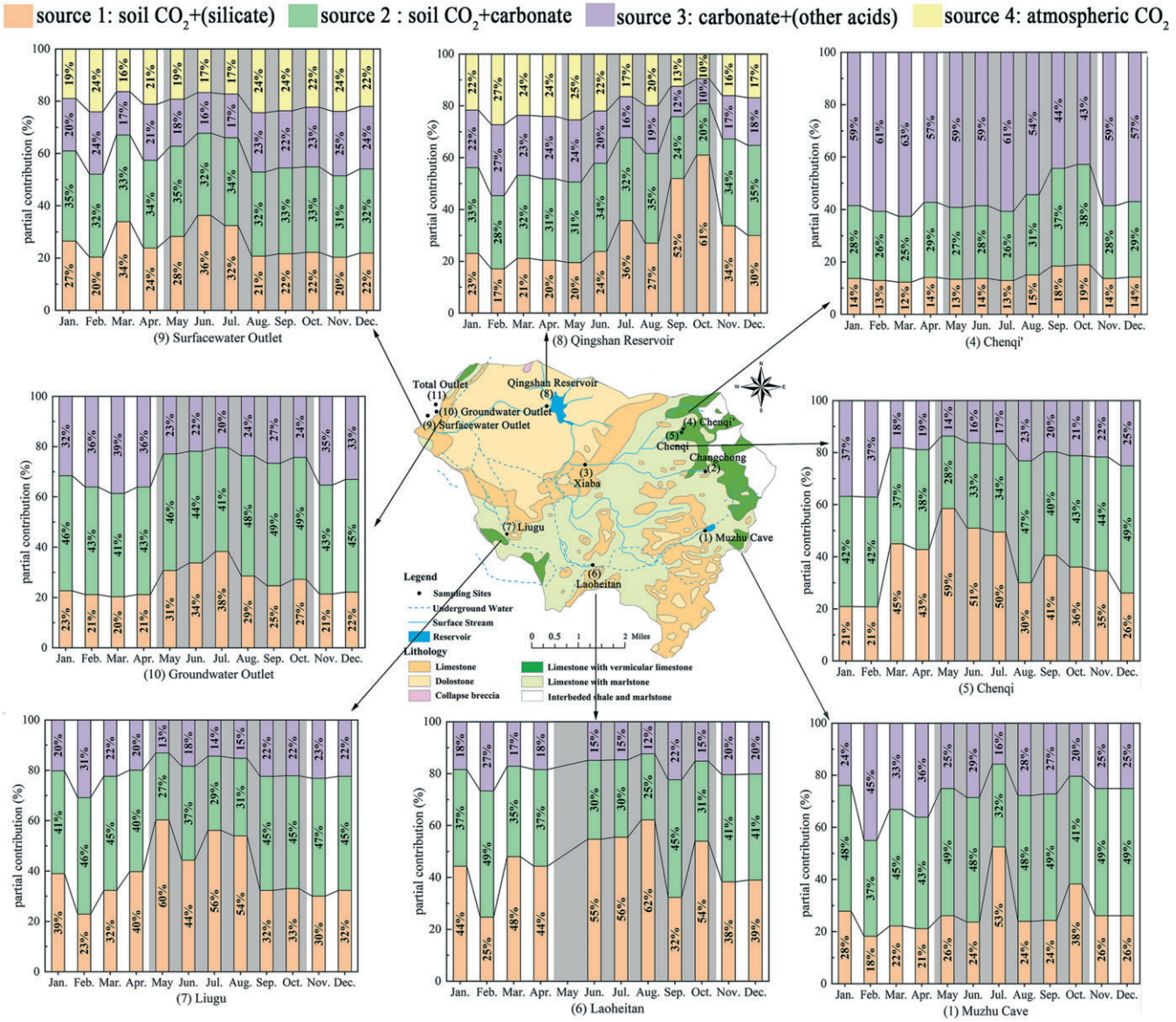

Figure 8. 100% stacked column showing spatiotemporal variations of source contributions to DIC. This graph only shows eight sampling sites in order to clearly display the change from upper stream to the lower reaches of the Houzhai catchment, and the other sites have a similar trend. Note Source 4, which was only for Nos 8 and 9 (both belong to the surface stream). The shaded background stands for high-flow months. This figure shows the results of the mixing model IsoSource, indicating that DIC in most underground water comes mainly from soil CO_2 or/and its reaction with carbonate (except for site No. 4). The meteorological factors in the wet season can affect the respective contribution of different sources to DIC, thus leading to a wider fluctuation in high-flow months than in low-flow months. During the wet season, soil CO_2 is the primary contributor to DIC at both UGW and SFS. The only exception is site No. 4, where the $CaCO_3$ was the dominant source (also during the dry season). [Colour figure can be viewed at wileyonlinelibrary.com]

information about soil water and hydrology (e.g. soil moisture and discharge). These hypotheses about how hydrological variations affect carbon dynamics still remain unanswered and need to be resolved further.

As shown in Figure 9, the higher discharge in the wet season (especially during the storm on 9 June) resulted in increases in both TDS (a proxy for carbonate weathering) and DIC loads, but decreases in $\delta^{13}C_{DIC}$ values. This finding provided strong evidence supporting the view that a high discharge in the wet season tends to dissolve more soil CO_2 and then favours carbonate weathering, and the increased amount of DIC in the wet season was mostly contributed by ^{12}C-enriched soil CO_2 instead of ^{13}C-enriched $CaCO_3$. The influence of the storm on 9 June will be discussed further in later sections. However, it should be noted that all monthly sampling campaigns were carried out on non-rain days; thus, the monthly discharges and loads in Figure 9 were instantaneous values at the instant of sampling, which cannot be used to calculate corresponding monthly or annual discharges in order to estimate corresponding parameter loads.

Therefore, conducting high-frequency sampling campaigns (e.g. hours) at only one or two sites, especially during the wet season, is necessary for the next work to more accurately estimate fluxes and model carbon dynamics in the K-CZ under diverse hydrological conditions using matching hydrological parameters (e.g. discharge and soil moisture obtained from *in-situ* sensors every 15/30 min).

In addition, the retained water in soil/karst matrix stored during the non-rain period also exerted a certain influence on $\delta^{13}C_{DIC}$ through permeation during rain events, while the extent of this possibly varies at different stages of the wet season but remains unknown.

Because many processes – including CO_2 exchange at the air–water interface, carbonate dissolution/deposition and

Table II. The contributions of original end-members to DIC at the 11 sampling sites of the Houzhai catchment (%)

Season	End-members	Sampling sites										
		No. 1	No. 2	No. 3	No. 4	No. 5	No. 6	No. 7	No. 8	No. 9	No. 10	No. 11
Wet	$CaCO_3$	46.3	46.7	41.9	69.0	37.1	32.1	35.5	31.2	36.0	46.4	49.3
	soil CO_2	53.7	53.3	58.1	31.0	62.9	67.9	64.5	51.1	43.4	53.6	50.7
	atm. CO_2								17.7	20.6		
Dry	$CaCO_3$	53.9	58.8	50.1	72.8	47.3	40.2	45.2	38.1	38.1	56.9	57.9
	soil CO_2	46.1	41.2	49.9	27.2	52.7	59.8	54.8	40.3	40.8	43.1	42.1
	atm. CO_2								21.6	21.1		

uptake of carbon by photosynthesis – can lead to isotope fractionation (Telmer and Veizer, 1999; Wachniew, 2006; Shin *et al.*, 2011; Dang *et al.*, 2018) and thus bring uncertainties to the above estimation, more detailed studies are urgently needed to reduce these uncertainties.

Enhanced carbon dynamics by rainstorms

An extra sampling campaign was conducted on 9 June 2013 when there was a daily rainfall of 55.8 mm, before the monthly sampling on 21 June 2013. In order to uncover the differences in parameters between the two field campaigns in June, *f*(P) (%) was introduced with the following calculating equation:

$$f\,(\mathrm{P}) = (\mathrm{P}_9 - \mathrm{P}_{21})/|\mathrm{P}_{21}|*100\% \quad (6)$$

where P_9 and P_{21} refer to a certain parameter (P) of samples collected on 9 June and 21 June, respectively, and$|P_{21}|$means absolute values of P_{21} considering the existence of negative values for log pCO_2 and $\delta^{13}C_{DIC}$.

Three patterns of value range about *f*(P) are shown in Figure 10 based on the reference datum of 0%. Firstly, *f* (NO_3^-), *f*(K^+) and *f* (DOC) showed varying degrees at different sampling sites and most were above 0%. This finding was generally attributed to the accelerated loss of chemical fertilizers or manure, because torrential rain, especially during farming activities, could lead to rapid leaching and oozing processes in this agricultural karstic region with only a thin soil layer (Yue *et al.*, 2018), the effect of which surpassed the impact of dilution caused by runoff under this degree of rainfall. However, this relationship between the two impacts is likely to change with the amount of rain and its intensity. In addition, the influence of eluviation largely depended on the land use and hydraulic connective (Ding *et al.*, 2011; Zhang *et al.*, 2017), thus these *f*(P) values were dissimilar at the 11 sampling sites. For example, site No. 4 had a deeper base flow and thus suffered less anthropogenic disturbance, leading to relatively small *f*(P) values compared to most remaining sites, which were surrounded by more agriculture or villages. Site No. 8 (fed by reservoir) belonged to surface water with longer impoundment time and the parameters here were comparatively steady with just a minor fluctuation between the two sampling campaigns because of high water volumes which caused a degree of buffering.

By contrast, the *f*(P) values of other ions, including SO_4^{2-}, Cl^-, Mg^{2+} and Na^+, were under 0% at most sampling sites. This observation might be explained by the limited increment of these ions during the big storm event in which the increased flow generated a dilution effect. In addition, slightly negative values of *f* (log pCO_2) in most phreatic aquifers might be ascribed to the consumption of soil CO_2 by carbonate dissolution or weak CO_2 degassing from conduit outlets resulting from turbulence during rainfall pulses, and there was not a large enough supplement of additional CO_2 along the flow pathway to offset this depletion (McClanahan *et al.*, 2016).

However, *f*(P) of HCO_3^- and Ca^{2+} was close to 0%, revealing their stabilization after a 55.8 mm storm. Dissolved soil CO_2 could compensate [HCO_3^-]; and attendant carbonate dissolution aroused by groundwater was likely to contribute additional ion content with flow, only just offsetting the relevant dilution under this extent of rainfall (Szramek *et al.*, 2007, 2011; Maher, 2011). This phenomenon corresponded to the range of *f* (log pCO_2) and also provided one interpretation as to why the data of *f* (DIC) were also approximately 0% and why *f*($\delta^{13}C_{DIC}$) fell in the grey shaded area. Among these sampling sites, Nos 1, 2 and 8 have more negative values of *f*($\delta^{13}C_{DIC}$), at −38, −34 and −47%, respectively, indicating that the stable carbon isotopes in these three sites were more susceptible to rainstorms. Groundwater has enough retention time to interact with carbonate minerals before the rain event and will be extruded eventually by downward percolating stormwater. The infiltration process during the storm period is too short as a result of the highly transmissive karst structure and thus mostly carries biogenic carbon, such as diffused soil CO_2, instead of geological carbon from carbonate rocks, leading to more ^{13}C-depleted DIC existing in the fluid (Figure 7). Furthermore, sites No. 1 and 2 are in the upper reaches, with many peak-cluster depressions encircled by karst mountainous peaks and widespread sinkholes (Zhang *et al.*, 2017), so just local seepage of rainwater can replenish the underground conduit during rainstorms, and there is faster leakage and a mixture of surface and groundwater, resulting in a bigger difference in $\delta^{13}C_{DIC}$ between the rain and non-rain periods. Site No. 8 is an open reservoir where pCO_2 tends to be balanced with the overlying atmosphere, so DIC here was relatively enriched in ^{13}C during the dry season. However, when a sudden rainstorm takes place, more ^{13}C-depleted DIC, carried by subterranean water along the pathway, will flow into this reservoir. The turbulence and input of excess DIC may enable some inherent CO_2 to escape from the water, and there is insufficient time to exchange CO_2 between the surface water and ambient air, resulting in an abrupt decline in $\delta^{13}C_{DIC}$. The *f*($\delta^{13}C_{DIC}$) of site No. 4 was close to 0% and this is possibly explained by its stable hydrological environment, which was not easily disturbed by external meteorological conditions. However, a stronger storm might cause a bigger change. *f*($\delta^{13}C_{DIC}$) in the middle reaches was slightly negative, perhaps because more water could be received during a rain event from upstream or surrounding springs, which dissolved more soil CO_2 and gave enough time in contact with carbonates during transit to produce a mixed carbon isotopic signal in the water. As for *f* (TDS), its composed status was perhaps related to the combined influence of ions as already mentioned. In general, the upper reaches of this catchment are more susceptible to rainstorms and, compared with UGW, SFS can respond more quickly to overland runoff during rain events.

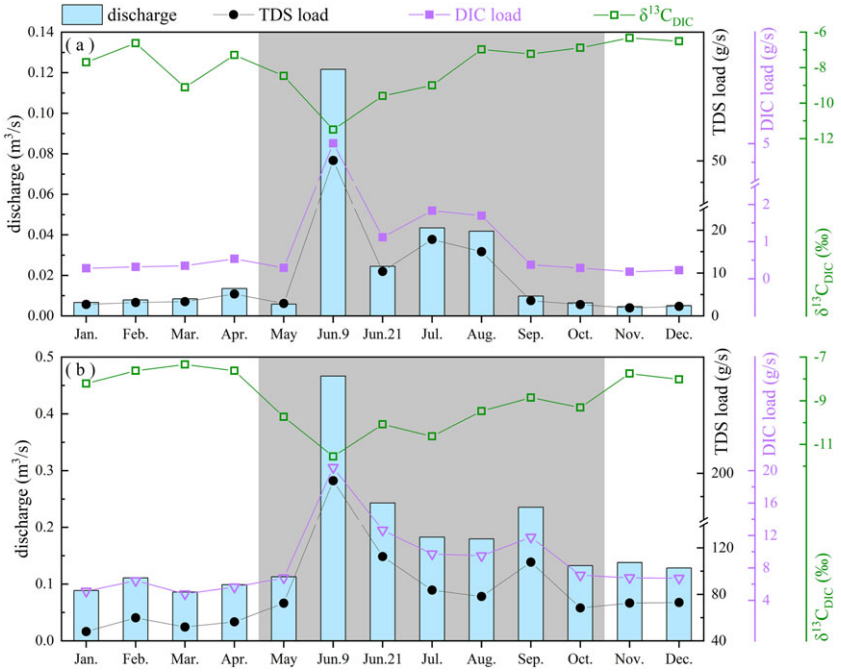

Figure 9. Instantaneous discharge and corresponding loads at the instant of monthly sampling at (a) site No. 9 (the outlet of surface water) and (b) site No. 10 (the outlet of groundwater). The shaded background stands for the wet season. Jun. 9 and Jun. 21 refer to the dates of two sampling campaigns in June, on 9 June (one storm) and 21 June (monthly sampling of June), respectively. This figure shows that when higher discharge in the wet season (especially from June to September) increases both TDS (a proxy for carbonate weathering) and DIC loads, it also simultaneously lowers $\delta^{13}C_{DIC}$ values, providing strong evidence supporting the fact that the increased amount of DIC in the wet season was mostly contributed by ^{12}C-enriched soil CO_2, instead of ^{13}C-enriched $CaCO_3$. [Colour figure can be viewed at wileyonlinelibrary.com]

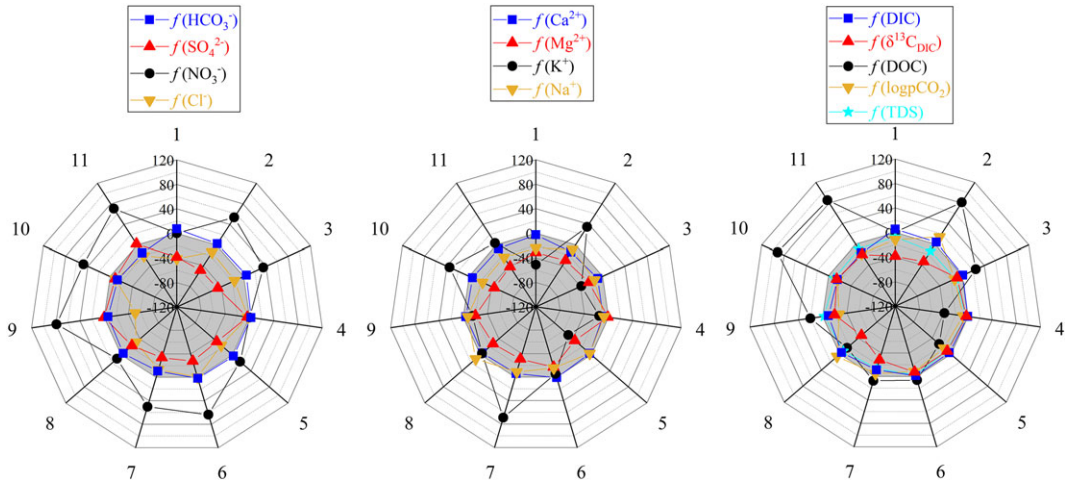

Figure 10. Radar plots of $f(P)$ (%) reflecting the influence of rain event on some parameters of water at 11 sampling sites. $f(P)$ (%) = $(P_9 - P_{21})/|P_{21}|$* 100%, indicating the variation degree of a certain parameter (P) after rainfall relative to normal circumstances. P refers to the concentrations of the main ions, TDS, DOC and DIC, as well as log pCO_2 and $\delta^{13}C_{DIC}$. The grey shaded area stands for negative values of $f(P)$ ranging from −120 to 0%. The numbers around the radar circles represent the corresponding ID of sampling sites. This figure indicates that rainstorms are a significant controlling factor for both hydrochemistry and DIC biogeochemical processes in the karstic catchment, with highly transmissive karst structure. There are different responses for diverse parameters to rainstorms. [Colour figure can be viewed at wileyonlinelibrary.com]

Unfortunately, there are no records of rain amounts or discharges during this storm at sampling sites, so it is impossible to calculate the fluxes accurately and to deduce the respective contributions to the total outlet of the whole basin. In addition, diverse rain intensity and rainfall could impose different impacts on hydrochemical processes and carbon fates, which might be why the relationship of parameters between these two sampling activities was inconsistent to some extent with regard to the relationship of data between 2007 and 2013. This hypothesis still remains unclear and needs to be resolved further. In addition, it is also difficult to conclude the quantitative relationship between rain amounts and carbonate weathering based only on this one rain event, so this will be a key point for future study.

Conclusions

This research is one of the first studies to systematically describe the spatiotemporal patterns of both DIC concentrations and its dominant sources and to elucidate relevant controlling factors by means of hydrochemistry and carbon isotopes in a small representative karstic catchment in Southwestern China. In this study, DIC concentrations ranged from 2.52 to

5.85 mmol l^{-1} (mean 4.15 mmol l^{-1}) and were higher in UGW than in SFS. Compared with other dissolved solutes, DIC concentrations showed a minor temporal fluctuation (especially in the middle and lower reaches) and an inconsistent seasonal trend (higher in the wet season than in the dry season at some sites), caused by the buffering of inputs from biogenic CO_2 dissolution and carbonate weathering, especially in the wet season because of higher bio-production and more rainfall.

$\delta^{13}C$ of DIC ($\delta^{13}C_{DIC}$) varied from −15.7 to −4.5‰ (mean −9.6‰) with significant spatial and seasonal variations (i.e. lower in the wet season than in the dry season at each site, and higher in UGW than in SFS). This pattern is relevant to the spatio-temporal changes of DIC sources. During the dry season, DIC mainly originated from ^{13}C-enriched $CaCO_3$ at most UGW sites (excluding in the middle reaches). During the wet season, ^{13}C-depleted soil CO_2 was the primary contributor to DIC in both UGW and SFS, and was higher than in the dry season at each sampling site, partially because of the influence of climate factors (e.g. rainfall and temperature), the change of dominant flow (i.e. slow base flow through tiny fissures/matrix or quick flow through large fractures/conduits) and agricultural activities (the application of fertilizer/manure). The contribution of atmospheric CO_2 to DIC could be ignored for UGW but should be considered for SFS. In addition, dedolomitization might also be a regulator of DIC in a deep confined spring draining gypsum stratum.

Overall, DIC concentrations and its sources in the karst catchments were controlled by many factors, including climate (rainfall and temperature), soil CO_2, water flow path/types, human activities (the usage of fertilizer/manure) and other processes (e.g. carbonate weathering and dedolomitization). In addition, this study provides strong evidence supporting the fact that DIC dynamics could be enhanced by rainstorms. Therefore, high temporal resolution information during storms and more in-depth analyses are necessary in the future to understand those processes and mechanisms and to estimate carbon fluxes more accurately in the karstic critical zone, and then to provide detailed cognition about carbon fate and relevant biogeochemical processes.

Acknowledgements—The National Natural Science Foundation of China (No. 41571130072 and No. 41203090) and the Ministry of Science and Technology of the People's Republic of China (National Key R&D Programme# 2016YFA0601002) jointly funded this research. Professor Robert M. Ellam and Mr John Thompson carried out English text editing. Dr Qiang-Sheng Huang and Wei-Qi Lu participated in the sample collections.

References

Amiotte-Suchet P, Aubert D, Probst JL, Gauthier-Lafaye F, Probst A, Andreux F, Viville D. 1999. $\delta^{13}C$ pattern of dissolved inorganic carbon in a small granitic catchment: the Strengbach case study (Vosges mountains, France). *Chemical Geology* **159**(1): 129–145. https://doi.org/10.1016/S0009-2541(99)00037-6.

Amiotte-Suchet P, Probst J-L, Ludwig W. 2003. Worldwide distribution of continental rock lithology: implications for the atmospheric/soil CO_2 uptake by continental weathering and alkalinity river transport to the oceans. *Global Biogeochemical Cycles* **17**(2): 1038): 7/1–7/13. https://doi.org/10.1029/2002gb001891.

Appelo CAJ, Postma D. 2005. *Geochemistry, Groundwater and Pollution*, 2nd edn. A.A. Balkema: Leiden.

Atekwana EA, Krishnamurthy RV. 1998. Seasonal variations of dissolved inorganic carbon and $\delta^{13}C$ of surface waters: application of a modified gas evolution technique. *Journal of Hydrology* **205**(3): 265–278. https://doi.org/10.1016/S0022-1694(98)00080-8.

Bowes MJ, House WA, Hodgkinson RA, Leach DV. 2005. Phosphorus-discharge hysteresis during storm events along a river catchment: the River Swale, UK. *Water Research* **39**(5): 751–762. https://doi.org/10.1016/j.watres.2004.11.027.

Cai W-J, Guo X, Chen C-TA, Dai M, Zhang L, Zhai W, Lohrenz SE, Yin K, Harrison PJ, Wang Y. 2008. A comparative overview of weathering intensity and HCO_3^- flux in the world's major rivers with emphasis on the Changjiang, Huanghe, Zhujiang (Pearl) and Mississippi Rivers. *Continental Shelf Research* **28**(12): 1538–1549. https://doi.org/10.1016/j.csr.2007.10.014.

Cai Y, Guo L, Wang X, Aiken G. 2015. Abundance, stable isotopic composition, and export fluxes of DOC, POC, and DIC from the Lower Mississippi River during 2006–2008. *Journal of Geophysical Research: Biogeosciences* **120**(11): 2273–2288. https://doi.org/10.1002/2015jg003139.

Calabrese S, Parolari AJ, Porporato A. 2017. Hydrologic transport of dissolved inorganic carbon and its control on chemical weathering. *Journal of Geophysical Research: Earth Surface* **122**(10): 2016–2032. https://doi.org/10.1002/2017jf004346.

Calmels D, Gaillardet J, Brenot A, France-Lanord C. 2007. Sustained sulfide oxidation by physical erosion processes in the Mackenzie River basin: climatic perspectives. *Geology* **35**(11): 1003. https://doi.org/10.1130/g24132a.1.

Calmels D, Gaillardet J, François L. 2014. Sensitivity of carbonate weathering to soil CO_2 production by biological activity along a temperate climate transect. *Chemical Geology* **390**: 74–86. https://doi.org/10.1016/j.chemgeo.2014.10.010.

Cerling TE, Solomon DK, Quade J, Bowman JR. 1991. On the isotopic composition of carbon in soil carbon dioxide. *Geochimica et Cosmochimica Acta* **55**: 3403–3405.

Chen HY, Chen BY, Chen B. 2005. Lithologic characteristics of Houzhai karst small valley. *Puding, Guizhou Province. Guizhou Geology* **22**: 284–288 in Chinese.

Chen X, Chen C, Hao Q, Zhang Z, Shi P. 2008. Simulation of rainfall-underground outflow responses of a karstic watershed in Southwest China with an artificial neural network. *Water Science and Engineering* **1**(2): 1–9. https://doi.org/10.3882/j.issn.1674-2370.2008.02.001.

Clark ID, Fritz P. 1997. *Environmental Isotopes in Hydrogeology*. Lewis Publishers: New York.

Clow DW, Mast MA. 2010. Mechanisms for chemostatic behavior in catchments: implications for CO_2 consumption by mineral weathering. *Chemical Geology* **269**(1&2): 40–51. https://doi.org/10.1016/j.chemgeo.2009.09.014.

Cuntz M. 2011. Carbon cycle: a dent in carbon's gold standard. *Nature* **477**: 547–548. https://doi.org/10.1038/477547a.

Dang DH, Evans RD, Durrieu G, Layglon N, El Houssainy A, Mullot JU, Lenoble V, Mounier S, Garnier C. 2018. Quantitative model of carbon and nitrogen isotope composition to highlight phosphorus cycling and sources in coastal sediments (Toulon Bay, France). *Chemosphere* **195**: 683–692. https://doi.org/10.1016/j.chemosphere.2017.12.109.

Dianwu Z, Seip HM. 1991. Assessing effects of acid deposition in Southwestern China using the magic model. *Water, Air, and Soil Pollution* **60**(1): 83–97. https://doi.org/10.1007/BF00293967.

Ding H, Lang Y-C, Liu C-Q. 2011. The impact of land use and land cover changes on solute dynamics in seepage water of soil from karst hillslopes of Southwest China. *Applied Geochemistry* **26**: S183–S186. https://doi.org/10.1016/j.apgeochem.2011.03.098.

Donnini M, Frondini F, Probst J-L, Probst A, Cardellini C, Marchesini I, Guzzetti F. 2016. Chemical weathering and consumption of atmospheric carbon dioxide in the Alpine region. *Global and Planetary Change* **136**: 65–81. https://doi.org/10.1016/j.gloplacha.2015.10.017.

Dreybrodt W. 1988. *Processes in Karst Systems*. Springer: Heidelberg.

Ford D, Williams P. 2013. *Karst Hydrogeology and Geomorphology*. Wiley: Chichester.

Gaillardet J, Calmels D, Romero-Mujalli G, Zakharova E, Hartmann J. 2018. Global climate control on carbonate weathering intensity. *Chemical Geology* (in press. https://doi.org/10.1016/j.chemgeo.2018.05.009.

Han G, Liu C-Q. 2004. Water geochemistry controlled by carbonate dissolution: a study of the river waters draining karst-dominated terrain, Guizhou Province, China. *Chemical Geology* **204**(1&2): 1–21. https://doi.org/10.1016/j.chemgeo.2003.09.009.

Hartmann J, Jansen N, Dürr HH, Kempe S, Köhler P. 2009. Global CO_2-consumption by chemical weathering: what is the contribution of highly active weathering regions? *Global and Planetary Change* **69**(4): 185–194. https://doi.org/10.1016/j.gloplacha.2009.07.007.

Hélie J-F, Hillaire-Marcel C, Rondeau B. 2002. Seasonal changes in the sources and fluxes of dissolved inorganic carbon through the St. Lawrence River—isotopic and chemical constraint. *Chemical Geology* **186**(1): 117–138. https://doi.org/10.1016/S0009-2541(01)00417-X.

Ilstedt U, Nordgren A, Malmer A. 2000. Optimum soil water for soil respiration before and after amendment with glucose in humid tropical acrisols and a boreal mor layer. *Soil Biology & Biochemistry* **32**(11&12): 1591–1599. https://doi.org/10.1016/S0038-0717(00)00073-0.

Jiang Y. 2013. The contribution of human activities to dissolved inorganic carbon fluxes in a karst underground river system: evidence from major elements and $\delta^{13}C_{DIC}$ in Nandong, Southwest China. *Journal of Contaminant Hydrology* **152**: 1–11. https://doi.org/10.1016/j.jconhyd.2013.05.010.

Jiang H, Liu W, Zhao T, Sun H, Xu Z. 2018. Water geochemistry of rivers draining karst-dominated regions, Guangxi province, South China: implications for chemical weathering and role of sulfuric acid. *Journal of Asian Earth Sciences* **163**: 152–162. https://doi.org/10.1016/j.jseaes.2018.05.017.

Lerman A, Wu L, Mackenzie FT. 2007. CO_2 and H_2SO_4 consumption in weathering and material transport to the ocean, and their role in the global carbon balance. *Marine Chemistry* **106**(1&2): 326–350. https://doi.org/10.1016/j.marchem.2006.04.004.

Li S-L, Calmels D, Han G, Gaillardet J, Liu C-Q. 2008. Sulfuric acid as an agent of carbonate weathering constrained by $\delta^{13}C_{DIC}$: examples from Southwest China. *Earth and Planetary Science Letters* **270**(3&4): 189–199. https://doi.org/10.1016/j.epsl.2008.02.039.

Li S-L, Liu C-Q, Li J, Lang Y-C, Ding H, Li L. 2010. Geochemistry of dissolved inorganic carbon and carbonate weathering in a small typical karstic catchment of Southwest China: isotopic and chemical constraints. *Chemical Geology* **277**(3&4): 301–309. https://doi.org/10.1016/j.chemgeo.2010.08.013.

Li S-L, Liu C-Q, Li J, Xue Z, Guan J, Lang Y, Ding H, Li L. 2013. Evaluation of nitrate source in surface water of southwestern China based on stable isotopes. *Environmental Earth Sciences* **68**(1): 219–228. https://doi.org/10.1007/s12665-012-1733-9.

Maher K. 2011. The role of fluid residence time and topographic scales in determining chemical fluxes from landscapes. *Earth and Planetary Science Letters* **312**(1&2): 48–58. https://doi.org/10.1016/j.epsl.2011.09.040.

Marwick TR, Tamooh F, Teodoru CR, Borges AV, Darchambeau F, Bouillon S. 2015. The age of river-transported carbon: a global perspective. *Global Biogeochemical Cycles* **29**: 122–137. https://doi.org/10.1002/2014GB004911.

McClanahan K, Polk J, Groves C, Osterhoudt L, Grubbs S. 2016. Dissolved inorganic carbon sourcing using $\delta^{13}C_{DIC}$ from a karst influenced river system. *Earth Surface Processes and Landforms* **41**(3): 392–405. https://doi.org/10.1002/esp.3856.

Perrin A-S, Probst A, Probst J-L. 2008. Impact of nitrogenous fertilizers on carbonate dissolution in small agricultural catchments: implications for weathering CO_2 uptake at regional and global scales. *Geochimica et Cosmochimica Acta* **72**(13): 3105–3123. https://doi.org/10.1016/j.gca.2008.04.011.

Plummer LN, Busenberg E. 1982. The solubilities of calcite, aragonite and vaterite in CO_2–H_2O solutions between 0 and 90°C, and an evaluation of the aqueous model for the system $CaCO_3$–CO_2–H_2O. *Geochimica et Cosmochimica Acta* **46**(6): 1011–1040. https://doi.org/10.1016/0016-7037(82)90056-4.

Pu J, Li J, Khadka MB, Martin JB, Zhang T, Yu S, Yuan D. 2017. In-stream metabolism and atmospheric carbon sequestration in a groundwater-fed karst stream. *Science of the Total Environment* **579**: 1343–1355. https://doi.org/10.1016/j.scitotenv.2016.11.132.

Regnier P, Friedlingstein P, Ciais P, Mackenzie FT, Gruber N, Janssens IA, Laruelle GG, Lauerwald R, Luyssaert S, Andersson AJ, Arndt S, Arnosti C, Borges AV, Dale AW, Gallego-Sala A, Goddéris Y, Goossens N, Hartmann J, Heinze C, Ilyina T, Joos F, LaRowe DE, Leifeld J, Meysman FJR, Munhoven G, Raymond PA, Spahni R, Suntharalingam P, Thullner M. 2013. Anthropogenic perturbation of the carbon fluxes from land to ocean. *Nature Geoscience* **6**: 597. https://doi.org/10.1038/ngeo1830.

Romero-Mujalli G, Hartmann J, Börker J, Gaillardet J, Calmels D. 2018. Ecosystem controlled soil-rock pCO_2 and carbonate weathering – constraints by temperature and soil water content. *Chemical Geology* (in press. https://doi.org/10.1016/j.chemgeo.2018.01.030.

Schulte P, van Geldern R, Freitag H, Karim A, Négrel P, Petelet-Giraud E, Probst A, Probst J-L, Telmer K, Veizer J, Barth JAC. 2011. Applications of stable water and carbon isotopes in watershed research: weathering, carbon cycling, and water balances. *Earth-Science Reviews* **109**(1&2): 20–31. https://doi.org/10.1016/j.earscirev.2011.07.003.

Semhi K, Suchet P, Clauer N, Probst J-L. 2000. Impact of nitrogen fertilizers on the natural weathering-erosion processes and fluvial transport in the Garonne basin. *Applied Geochemistry* **15**(6): 865–878.

Shin WJ, Chung GS, Lee D, Lee KS. 2011. Dissolved inorganic carbon export from carbonate and silicate catchments estimated from carbonate chemistry and $\delta^{13}C_{DIC}$. *Hydrology and Earth System Sciences* **15**(8): 2551–2560. https://doi.org/10.5194/hess-15-2551-2011.

Song X, Gao Y, Wen X, Guo D, Yu G, He N, Zhang J. 2017. Carbon sequestration potential and its eco-service function in the karst area, China. *Journal of Geographical Sciences* **27**(8): 967–980. https://doi.org/10.1007/s11442-017-1415-3.

Szramek K, McIntosh JC, Williams EL, Kanduc T, Ogrinc N, Walter LM. 2007. Relative weathering intensity of calcite versus dolomite in carbonate-bearing temperate zone watersheds: carbonate geochemistry and fluxes from catchments within the St. Lawrence and Danube river basins. *Geochemistry, Geophysics, Geosystems* **8**(4). https://doi.org/10.1029/2006gc001337.

Szramek K, Walter LM, Kanduč T, Ogrinc N. 2011. Dolomite versus calcite weathering in hydrogeochemically diverse watersheds established on bedded carbonates (Sava and Soča rivers, Slovenia). *Aquatic Geochemistry* **17**(4&5): 357–396. https://doi.org/10.1007/s10498-011-9125-4.

Telmer K, Veizer J. 1999. Carbon fluxes, pCO_2 and substrate weathering in a large northern river basin, Canada: carbon isotope perspectives. *Chemical Geology* **159**(1): 61–86. https://doi.org/10.1016/S0009-2541(99)00034-0.

Tian L-Y, Lang Y-C, Liu C-Q, Ding H, Zhao Z-Q, Liu T-Z. 2013. Distribution patterns of organic carbon and its isotope compositions in soil profiles on the slopes in Puding karst areas of Guizhou Province, Southwest China. *Chinese Journal of Ecology* **32**(9): 2362–2367 (in Chinese. https://doi.org/10.13292/j.1000-4890.2013.0329.

Torres MA, Moosdorf N, Hartmann J, Adkins JF, West AJ. 2017. Glacial weathering, sulfide oxidation, and global carbon cycle feedbacks. *Proceedings of the National Academy of Sciences* **114**: 8716–8721.

Vogel JC. 1993. 4-Variability of carbon isotope fractionation during photosynthesis. In *Stable Isotopes and Plant Carbon–Water Relations*, Ehleringer JR, Hall AE, Farquhar GD (eds). Academic Press: San Diego, CA.

Voss BM, Peucker-Ehrenbrink B, Eglinton TI, Fiske G, Wang ZA, Hoering KA, Montluçon DB, LeCroy C, Pal S, Marsh S, Gillies SL, Janmaat A, Bennett M, Downey B, Fanslau J, Fraser H, Macklam-Harron G, Martinec M, Wiebe B. 2014. Tracing river chemistry in space and time: dissolved inorganic constituents of the Fraser River, Canada. *Geochimica et Cosmochimica Acta* **124**: 283–308. https://doi.org/10.1016/j.gca.2013.09.006.

Wachniew P. 2006. Isotopic composition of dissolved inorganic carbon in a large polluted river: the Vistula, Poland. *Chemical Geology* **233**(3&4): 293–308. https://doi.org/10.1016/j.chemgeo.2006.03.012.

Wu Q, Han G, Tao F, Tang Y. 2012. Chemical composition of rainwater in a karstic agricultural area, Southwest China: the impact of urbanization. *Atmospheric Research* **111**: 71–78. https://doi.org/10.1016/j.atmosres.2012.03.002.

Yang C, Telmer K, Veizer J. 1996. Chemical dynamics of the "St. Lawrence" riverine system: δD_{H2O}, $\delta^{18}O_{H2O}$, $\delta^{13}C_{DIC}$, $\delta^{34}S_{sulfate}$, and dissolved $^{87}Sr/^{86}Sr$. *Geochimica et Cosmochimica Acta* **60**(5): 851–866. https://doi.org/10.1016/0016-7037(95)00445-9.

Yang R, Liu Z, Zeng C, Zhao M. 2012. Response of epikarst hydrochemical changes to soil CO_2 and weather conditions at Chenqi, Puding, SW China. *Journal of Hydrology* **468/469**: 151–158. https://doi.org/10.1016/j.jhydrol.2012.08.029.

Yu Y, Liu C, Wang F, Wang B, Li J, Li S. 2008. Dissolved inorganic carbon and its isotopic differentiation in cascade reservoirs in the Wujiang drainage basin. *Chinese Science Bulletin* **53**(21): 3371–3378. https://doi.org/10.1007/s11434-008-0348-8.

Yuan DX, Cai G. 1988. *The Science of Karst Environment*. Chongqing Publishers: Chongqing (in Chinese).

Yuan DX, Zhang C. 2008. Karst dynamics theory in China and its practice. *Acta Geoscientica Sinica* **29**(03): 355–365 in Chinese.

Yue F-J, Li S-L, Liu C-Q, Lang Y-C, Ding H. 2015. Sources and transport of nitrate constrained by the isotopic technique in a karst catchment: an example from Southwest China. *Hydrological Processes* **29**(8): 1883–1893. https://doi.org/10.1002/hyp.10302.

Yue F-J, Li S-L, Zhong J, Liu J. 2018. Evaluation of factors driving seasonal nitrate variations in surface and underground systems of a karst catchment. *Vadose Zone Journal* **17**(1). https://doi.org/10.2136/vzj2017.04.0071.

Zhang J, Quay PD, Wilbur DO. 1995. Carbon isotope fractionation during gas–water exchange and dissolution of CO_2. *Geochimica et Cosmochimica Acta* **59**: 107–114.

Zhang Z, Chen X, Soulsby C. 2017. Catchment-scale conceptual modelling of water and solute transport in the dual flow system of the karst critical zone. *Hydrological Processes* **31**(19): 3421–3436. https://doi.org/10.1002/hyp.11268.

Zhong J, Li SL, Tao F, Ding H, Liu J. 2017a. Impacts of hydrologic variations on chemical weathering and solute sources in the Min River basin, Himalayan–Tibetan region. *Environmental Science and Pollution Research International* **24**(23): 19126–19137. https://doi.org/10.1007/s11356-017-9584-2.

Zhong J, Li SL, Tao F, Yue F, Liu CQ. 2017b. Sensitivity of chemical weathering and dissolved carbon dynamics to hydrological conditions in a typical karst river. *Scientific Report* **7**: 42944. https://doi.org/10.1038/srep42944.

Zhong J, Li SL, Cai HM, Yue FJ, Tao FX. 2018. The response of carbon geochemistry to hydrological events within an urban river, Southwestern China. *Geochemistry International* **56**(5): 462–473. https://doi.org/10.1134/S0016702918050099.